Preprints of the 21st IFAC World Congress (Virtual)
Berlin, Germany, July 12-17, 2020

Model Predictive Control for Wave Energy Converters: A Moving Window Blocking Approach

Juan Guerrero-Fernández * **Oscar J. González-Villarreal** *
John Anthony Rossiter * **Bryn Jones** *

* *Department of Automatic Control and Systems Engineering, University of Sheffield, UK (e-mail: j.guerrero@sheffield.ac.uk; ojgonzalezvillarreal1@sheffield.ac.uk; j.a.rossiter@sheffield.ac.uk; b.l.jones@sheffield.ac.uk)*

Abstract: Ocean wave energy is one of the most concentrated sources of renewable energy. However, until now it has not reached the economic feasibility required to be commercialised. To improve the efficiency of wave energy converters, several advanced control strategies have been proposed, including Model Predictive Control (MPC). Nevertheless, the computational burden of the underlying optimisation problem is a drawback of conventional (Full-Degree of Freedom, F-DoF) MPC, which typically limits its application for real-time control of systems. In this paper, a Moving Window Blocking (MWB) approach is proposed to speed-up the time required for each optimisation problem by reducing the number of decision variables using input parameterised solutions. Numerical simulation of a generic single device point absorber wave energy converter controlled by this scheme confirms the potential of this approach.

Keywords: Wave energy converters, Model predictive controller, Moving window blocking.

1. INTRODUCTION

Ocean wave energy is one of the most concentrated renewable energy sources, and its resources are vast in many countries around the globe (Sheng, 2019). The estimated worldwide potential of ocean wave power is 32 000 TW h (Mørk et al., 2010), which is more than the worldwide electricity consumption of about 25 721 TW h (International Energy Agency, 2019).

The development and implementation of wave energy converters (WEC) may have several benefits. Examples of the benefits range from individual benefits for the country such as increasing of their renewable energy matrix and guaranteeing energy supply diversity (Sheng, 2019), to global benefits by confronting the problems of climate change and the difficult challenge of reducing the dependency on conventional energy resources such as fossils or nuclear energy.

To date, wave energy technologies are technically immature for reliable and economical energy generation (Sheng, 2019). One of the biggest challenges is how to improve the efficiency of wave energy converters. To address this issue, several control strategies have been proposed to alter the dynamic behaviour of the device in order to maximise the extracted energy. *Model Predictive Control* (MPC) is a well-developed control strategy within academic and industry communities which takes into account constraints whilst optimising a given cost function (Faedo et al., 2017). Although MPC can have explicit offline solutions (H.J.Ferreau, H.G. Bock, 2008), this is not tractable for the WEC problem given the large amount of variation present in the wave excitation forces which are external disturbances to the optimisation. Thus, for this application, MPC requires an online solution where at each sampling time, solves an Optimal Control Problem (OCP) to produce an optimal control sequence, the first of which is applied to the plant as the control action (Li and Belmont, 2014). However, one of the drawbacks of MPC is the computational burden required to solve the OCP.

To reduce the computational burden of the optimisation, a popular approach is to use input-parameterisation techniques which allow to reduce the number of degrees of freedom of the optimisation. Several input-parameterisation have been proposed such as Laguerre Polynomials (Wang, 2004), as well as orthonormal parameterisations based on collocation points, typically referred as pseudospectral methods (Garcia-Violini and Ringwood, 2019).

In this paper, a *Moving Window Blocking* (MWB) MPC approach is proposed with the idea of reducing the computational time required to solve the OCP at each sampling time. The results of the simulations show a performance comparable with the performance when implementing the Full-Degree of Freedom (F-DoF) MPC strategy, and offer a better performance than the Generalised Predictive Control (GPC) strategy.

The remaining part of this paper is organised as follows: Section 2 presents the mathematical model for a generic WEC. F-DoF Model Predictive Control and a detailed description of the proposed Moving Window Blocking MPC approach is given in Section 3. The results of the simulations are presented in Section 4. Finally, the conclusions and future work are set out in Section 5.

2. WEC MODELLING

For the development of the mathematical model of a wave energy converter (WEC), a heaving semi-submerged sphere is considered as in Figure 1. The hydrodynamic model is developed from first principles. Applying Newton's second law to the partially submerged sphere, the dynamics of the sphere are described by:

$$m\,\ddot{z}(t) = F_g - \iint_{S(t)} P(t)\,\mathbf{n}\,\mathrm{d}S \; + F_{PTO}(t) \tag{1}$$

Where m is the floater mass, z is the vertical displacement of the body relative to its hydrostatic equilibrium position, F_g is the force due to gravity, $F_{PTO}(t)$ is the force exerted by the Power Take-Off systems (PTO) (controller input $u(t)$), $P(t)$ is the pressure on an element $\mathrm{d}S$ on the buoy wetted surface, $\mathbf{n}$ is a vector normal to the surface element, $\mathrm{d}S$ and S is the submerged wetted surface.

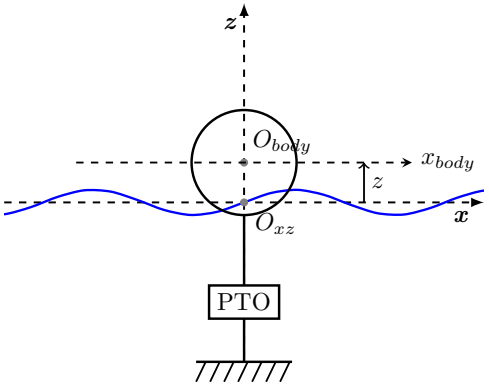

Fig. 1. A general wave energy converter with 1-DoF: heave

From (1), several models can be derived, depending on the complexity, computational time and accuracy desired. In this study, a linear hydrodynamic model is considered. For linear models, assuming the fluid is in-compressible, in-viscid and irrotational [1], (1) is typically solved using potential flow theory, in which the potential problem is linearised and computed around the position of equilibrium. Considering small displacements, and seabed as reference system, (1) is rewritten as follows:

$$m\,\ddot{z}(t) = F_{res}(t) + F_{rad}(t) + F_{exc}(t) + F_{PTO}(t), \tag{2}$$

where $F_{res}(t)$ is hydrostatic restoring force, $F_{rad}(t)$ is the radiation force, and $F_{exc}(t)$ the excitation force due to the incoming wave. The hydrostatic restoring force $F_{res}(t)$ represent the spring-like effect of the surrounding ocean water into the buoy, and is determined by k_h hydrostatic stiffness and $z(t)$ absorber position:

$$F_{res}(t) = -k_h\,z(t) \tag{3}$$

The excitation force $F_{exc}(t)$ describes the interactions between the incident waves and the body at its place of equilibrium, and is represented by the convolution of the excitation impulse response k_{exc} with the otherwise undisturbed free-surface elevation η at the centre of the body:

$$F_{exc}(t) = \int_{-\infty}^{t} k_{exc}(t-\tau)\,\eta(\tau)\,d\tau \tag{4}$$

[1] This is a standard assumption in the wave energy literature (Faedo et al., 2017).

Similarly, the radiation force $F_{rad}(t)$ is a damping/inertial force associated with waves radiated by the absorber oscillating in calm water scenario, and is expressed by the added mass μ_∞ and the convolution product between the radiation impulse response k_{rad} and the absorber velocity $\dot{z}(t)$:

$$F_{rad}(t) = -\mu_\infty\,\ddot{z}(t) - \int_{-\infty}^{t} k_{rad}(t-\tau)\,\dot{z}(\tau)\,d\tau \tag{5}$$

The convolution kernels k_{exc}, k_{rad} and the frequency-independent added mass μ_∞ are computed numerically using boundary element methods (BEMs). In this study the open source *NEMOH* (Penalba et al., 2017) was employed. Combining (3)-(5) with (2) gives the widely used equation (in WEC studies) Cummins' equation (Cummins, 1962):

$$\begin{aligned} m\,\ddot{z}(t) = &- k_h z(t) - \mu_\infty \ddot{z}(t) - \int_{-\infty}^{t} k_{rad}(t-\tau)\dot{z}(\tau)d\tau \\ &+ \int_{-\infty}^{t} k_{exc}(t-\tau)\eta(\tau)d\tau + F_{PTO}(t) \end{aligned} \tag{6}$$

At this point, a few statements can be made from (6). First, since the excitation force $F_{exc}(t)$ depends on the undisturbed free-surface elevation $\eta(t)$, it can be considered as an independent input to the system. Second, (6) is represented in state-space form for control strategy implementation and third, the direct computation of the convolution integral in (5) in time-domain simulation is computationally expensive and cumbersome (Roessling and Ringwood, 2015). To avoid the direct computation of the convolution integral at every time step, several methods to approximate the integral have been proposed (Yu and Falnes, 1995; Roessling and Ringwood, 2015; Pérez and Fossen, 2008). Approximating the convolution integral in (5) by a state-space system with the state vector $\underline{x_r}(t) \in \mathbb{R}^n$ is a common approach, where the input to the system is the velocity of the absorber ($v = \dot{z}$) and the approximation of the convolution integral term of the radiation force is the output:

$$\begin{aligned} \underline{\dot{x}_r}(t) &= A_r\,\underline{x_r}(t) + B_r\,\dot{z}(t) \\ \textstyle\int_{-\infty}^{t} k_{rad}(t-\tau)\dot{z}(\tau)\,d\tau &\approx C_r\,\underline{x_r}(t) \end{aligned} \tag{7}$$

This system is later included as a part of the overall model that describes the motion of the absorber. It is important to clarify that the system states in (7) have no physical meaning, but still contain information on the condition of the surrounding fluid (Cretel et al., 2011). In this study, the state space matrices A_r, B_r, and C_r were computed by the open source toolbox *FOAMM* (Finite Order Approximation by Moment-Matching, based on the theoretical foundations presented in Faedo et al. (2018)) Defining the state and output vectors, $\underline{x_c} \in \mathbb{R}^{n+2}$ and $\underline{y_c} \in \mathbb{R}^2$, for the linear time-invariant state-space system:

$$\underline{x_c} = \begin{bmatrix} z \\ \dot{z} \\ \underline{x_r} \end{bmatrix} \qquad \underline{y_c} = \begin{bmatrix} z \\ \dot{z} \end{bmatrix} \tag{8}$$

the whole dynamics of the WEC is given by:

$$\begin{aligned} \underline{\dot{x_c}}(t) &= A_c\,\underline{x_c}(t) + B_c\,F_{pto}(t) + B_c\,F_{exc}(t) \\ \underline{y_c}(t) &= C_c\,\underline{x_c}(t) \end{aligned} \tag{9}$$

in which $A_c \in \mathbb{R}^{(n+2)\mathrm{x}(n+2)}$, $B_c \in \mathbb{R}^{(n+2)\mathrm{x}1}$, $C_c \in \mathbb{R}^{2\mathrm{x}(n+2)}$, are defined as:

$$A_c=\begin{bmatrix} 0 & 1 & \mathbf{0} \\ \frac{-k_h}{m+\mu_\infty} & 0 & \frac{-C_r}{m+\mu_\infty} \\ \mathbf{0} & B_r & A_r \end{bmatrix};\ B_c=\begin{bmatrix} 0 \\ \frac{1}{m+\mu_\infty} \\ \mathbf{0} \end{bmatrix};\ C_c=\begin{bmatrix} 1 & 0 & \mathbf{0} \\ 0 & 1 & \mathbf{0} \end{bmatrix}$$

where $\mathbf{0}$ denotes a zero matrix of required dimensions.

By discretising system (9), and replacing F_{pto} and F_{exc} for u and u_{exc}, respectively, to use standard nomenclature, results in a general discrete state-space of the form.

$$\underline{x}_{k+1} = A_d\underline{x}_k + B_d\underline{u}_k + B_d\underline{u}_{exc_k} \tag{10a}$$
$$\underline{y}_k = C_d\underline{x}_k \tag{10b}$$

For this study, a discretisation of a zero-order hold was considered using a sampling time of $T_s = 0.1s$. The resulting state space matrices are given in section 4.

3. MODEL PREDICTIVE CONTROL

3.1 General Objective

In this paper, Model Predictive Control was used as general optimal control methodology with the general purpose of maximising the mechanical energy E_{abs} absorbed by the PTO system over a time horizon T, defined as:

$$E_{abs} = -\int_t^{t+T} u(\tau)\dot{z}(\tau)d\tau \tag{11}$$

Furthermore, real WEC systems will typically present position, input and input increments (slew rates) constraints related to physical limits which can be handled naturally by the MPC formulation. To benefit from the moving window blocking approach presented in subsection 3.4, this paper focuses particularly on the case where the WEC is within a "safe" operating region (i.e., operating within the position constraints, without making contact with the end-stops). Indeed, the device should be locked in a survival mode when exposed to extreme sea conditions (Sheng, 2019); this is reasonable given it is generally not possible to guarantee output feasibility (such as the buoy positions) for dynamics systems under significant disturbances. In simple terms, if a big enough wave is applied to the system, it would not even be possible to prevent it from reaching the limits, regardless of the input selection. An alternative might be to use soft-constraints for some output violations, however, this is out of the scope of this paper.

The discrete-time optimisation problem is thus chosen as:

$$minimise \quad J_k = \sum_{i=1}^{N_p} u_{k+i-1}\dot{z}_{k+i} \tag{12a}$$
$$s.t. \quad u_{min} \le u_{k+i-1} \le u_{max} \tag{12b}$$
$$\Delta u_{min} \le \Delta u_{k+i-1} \le \Delta u_{max} \tag{12c}$$

where N_p is the prediction horizon. Note that this cost considers the force u and velocity $\dot{z}$ at different time steps ($k+i-1$ and $k+i$). This is chosen to ensure causality of the solution as discussed in Li and Belmont (2014).

3.2 Predictions

Following the methodology described in Cretel et al. (2010), the state space model (10) is augmented with the previous input u_{k-1} to use the input increment Δu_k as the decision variable resulting in:

$$x_{k+1} = Ax_k + B\Delta u_k + B_w u_{exc_k} \tag{13a}$$
$$y_k = Cx_k \tag{13b}$$

where the state is now $x_k = [\underline{x}_k^T u_{k-1}]^T \in \mathbb{R}^{n+3}$, the output is $y_k = [\underline{y}_k^T u_{k-1}]^T \in \mathbb{R}^3$, and

$$A = \begin{bmatrix} A_d & B_d \\ \mathbf{0} & 1 \end{bmatrix} \quad B = \begin{bmatrix} B_d \\ 1 \end{bmatrix} \quad B_w = \begin{bmatrix} B_d \\ 0 \end{bmatrix} \quad C = \begin{bmatrix} C_d & \mathbf{0} \\ \mathbf{0} & 1 \end{bmatrix}$$

This change will allow simple expressions for input and input rate constraints, as well as the computation of the product $(u_{k+i-1}\dot{z}_k)$ through an appropriate matrix Q as discussed in Cretel et al. (2010, 2011). By propagating the model (13a) N_p times forward, all future outputs $\hat{Y} = [y_{k+1}^T, y_{k+2}^T, \cdots, y_{k+N_p}^T]^T \in \mathbb{R}^{3N_p}$ are given by:

$$\hat{Y} = Gx_k + H\Delta\hat{U} + H_w\hat{U}_w \tag{14}$$

where $\Delta\hat{U} = [\Delta\hat{u}_k, \Delta\hat{u}_{k+1}, \cdots, \Delta\hat{u}_{k+N_p}]^T \in \mathbb{R}^{N_p}$ are the future input increments; $\hat{U}_w = [\hat{u}_{w_k}, \hat{u}_{w_{k+1}}, \cdots, \hat{u}_{w_{k+N_p}}]^T \in \mathbb{R}^{N_p}$ are the future wave excitation forces; and matrices $G \in \mathbb{R}^{3N_p\times(n+3)}$ and $H \in \mathbb{R}^{3N_p\times N_p}$ are defined as:

$$G = \begin{bmatrix} CA \\ CA^2 \\ \vdots \\ CA^{N_p} \end{bmatrix}^T \qquad H = \begin{bmatrix} CB & \mathbf{0} & \cdots & \mathbf{0} \\ CAB & CB & \ddots & \vdots \\ \vdots & \ddots & \ddots & \mathbf{0} \\ CA^{N_p-1}B & \cdots & CAB & CB \end{bmatrix}$$

where $\mathbf{0}$ are zeros matrices with the same dimensions of CB, and H_w is defined as H using B_w instead.

3.3 Standard Optimisation

Having defined the prediction models, a standard quadratic cost function can be formulated as,

$$J = \frac{1}{2}\hat{Y}^T Q\hat{Y} \tag{15}$$

To compute the product $(u_{k-1}\dot{z}_k)$, the penalisation matrix $Q \in \mathbb{R}^{3N_p\times 3N_p}$ is selected as a block diagonal matrix with the inner matrices q_{k+i} defined as (Cretel et al., 2010),

$$Q = \begin{bmatrix} q_{k+1} & \mathbf{0} & \cdots & \mathbf{0} \\ \mathbf{0} & q_{k+2} & \ddots & \vdots \\ \vdots & \ddots & \ddots & \mathbf{0} \\ \mathbf{0} & \cdots & \mathbf{0} & q_{k+N_p} \end{bmatrix} \quad q_{k+i} = \begin{bmatrix} 0 & 0 & 0 \\ 0 & 0 & 1 \\ 0 & 1 & 0 \end{bmatrix} \quad \forall\, i = [1, N_p] \tag{16}$$

By substituting the output predictions (14) in (15), rearranging in terms of the decision variables ($\Delta\hat{U}$), and including input and input rate constraints, the standard quadratic program (17) is obtained.

$$J = \frac{1}{2}\Delta\hat{U}^T E\Delta\hat{U} + \Delta\hat{U}^T f \quad s.t. \quad M\Delta\hat{U} \le b \tag{17a}$$
$$E = H^T QH \qquad f = H^T Q(Gx_k + H_w\hat{U}_w) \tag{17b}$$
$$M = \begin{bmatrix} I \\ -I \\ D \\ -D \end{bmatrix} \qquad b = \begin{bmatrix} \Delta u_{max}\mathbf{1} \\ -\Delta u_{min}\mathbf{1} \\ (u_{max} - u_{k-1})\mathbf{1} \\ (-u_{min} + u_{k-1})\mathbf{1} \end{bmatrix} \tag{17c}$$

where $E \in \mathbb{R}^{N_p\times N_p}$ is a matrix known as the Hessian, here assumed to be positive definite; $f \in \mathbb{R}^{N_p}$ is a column-vector; $M \in \mathbb{R}^{4N_p\times N_p}$ is the constraint matrix; $b \in \mathbb{R}^{4N_p}$ is the constraint vector; $I \in \mathbb{R}^{N_p\times N_p}$ is an identity matrix;

$D \in \mathbb{R}^{N_p \times N_p}$ is a lower triangular matrix; and $\mathbf{1} \in \mathbb{R}^{N_p}$ column-vector is a column vector of ones.

Having defined E, f, M, b, the optimisation can then be solved using any QP solver such as quadprog function of Matlab, QP OASES (H.J.Ferreau, H.G. Bock, 2008), etc. At each sampling time, only the first input is applied to the system and the process is repeated at the next sampling time, which is the well known receding horizon control strategy.

3.4 Moving Window Blocking

In this paper, we used a blocking approach where the input is parameterised in blocks of size N_b having equal values, e.g. $u_k = u_{k+1} = \cdots = u_{k+N_b-1}$ for the first block, $u_{k+N_b} = u_{k+N_b+1} = \cdots = u_{k+2N_b-1}$ for the second block, etc., thus allowing the decision variables to be spread over the prediction horizon, as opposed to the standard Generalized Predictive Control (GPC) approach where the decision variable are "congested" at the beginning, and left constant after a "control horizon" (Rossiter, 2018). An example comparison of this is visualised in Fig. 2 for the WEC system defined in section 2, and is further discussed in the results section 4. This distinctive feature of the blocking approach is important for this application for two main reasons: firstly, the solution obtained from the original problem using full degrees of freedom applied to the WEC system is constantly saturated as seen in Fig. 2, thus can be accurately represented by blocks; and secondly, depending on the wave future values, it might be more important to have decisions available at the future, example when the wave reaches its crest and trough (maximum/minimum values).

The aforementioned blocking parameterisation can be achieved by defining a blocking matrix ($\mathbb{N}$) for the decision variables ($\Delta\hat{U}$) of the form:

$$\Delta\hat{U} = \mathbb{N}\Delta\hat{\mathbb{U}} \tag{18a}$$

$$\mathbb{N} = \begin{bmatrix} \mathbf{n} & \mathbf{0}_{N_b} & \cdots & \mathbf{0}_{N_b} \\ \mathbf{0}_{N_b} & \mathbf{n} & \ddots & \vdots \\ \vdots & \ddots & \ddots & \mathbf{0}_{\mathbf{N_b}} \\ \mathbf{0}_{N_b} & \cdots & \mathbf{0}_{N_b} & \mathbf{n} \end{bmatrix} \quad \mathbf{n} = \begin{bmatrix} 1 \\ \mathbf{0}_{N_b-1} \end{bmatrix} \tag{18b}$$

where $\hat{\mathbb{U}} \in \mathbb{R}^{N_u}$ are the blocked decision variables which have reduced dimensions of $N_u = \lceil \frac{N_p}{N_b} \rceil \mathbf{n} \in \mathbb{R}^{N_b}$, and $\mathbf{0}_v \in \mathbb{R}^v$ is a column-vector of v zeros. For simplicity, N_p should be selected as a multiple integer of the block size N_b, otherwise the last $\mathbf{n}$ in the diagonal might be different.

Moreover, as discussed in Cagienard et al. (2007), the application of standard blocking approaches has an inconsistent nature, and suffers from recursive feasibility problems given the decision in the previous time step cannot be replicated which is detrimental to the performance. To address this, the Moving Window Blocking (MWB) approach developed in Cagienard et al. (2007) proposed to shift the set of N_b admissible blocking matrices $\mathbb{N}_i$ along with the moving horizon resulting in an input parameterisation of the form.

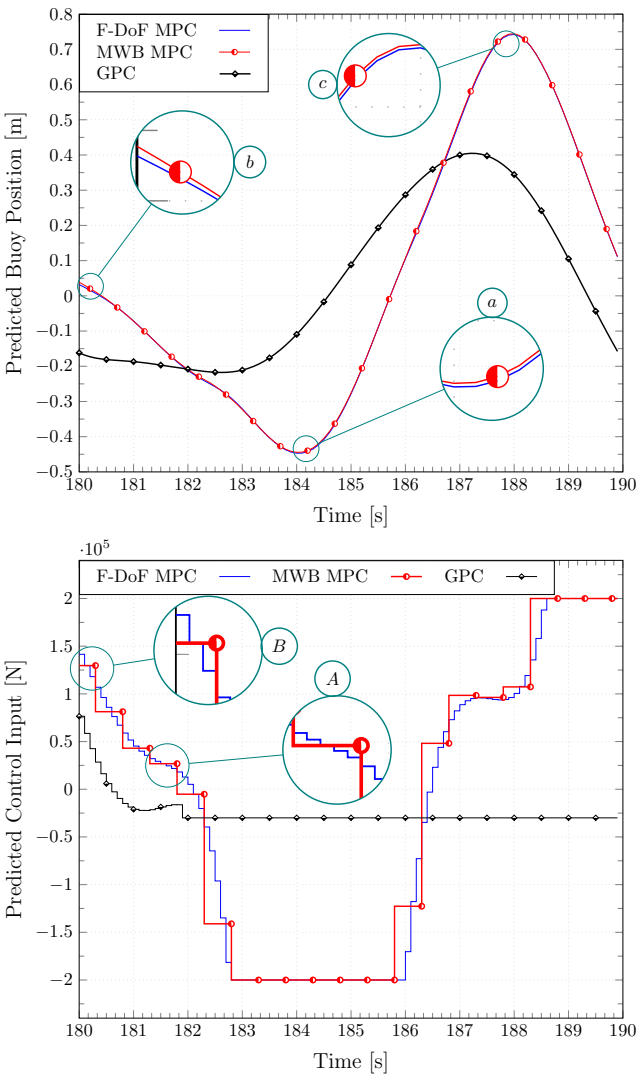

Fig. 2. Predicted Trajectories for Buoy Position z (upper plot) and Input u (lower plot).

$$\Delta\hat{U} = \mathbb{N}_i\Delta\hat{\mathbb{U}} \qquad \forall\, i = [1, N_b] \tag{19a}$$

$$\mathbb{N}_i = \begin{bmatrix} \mathbf{n}_1 & \mathbf{0}_{N_b-i} & \cdots & \mathbf{0}_{N_b-i} \\ \mathbf{0_{N_b}} & \mathbf{n} & \ddots & \vdots \\ \vdots & \ddots & \ddots & \mathbf{0}_{N_b} \\ \mathbf{0}_{N_b-2+i} & \cdots & \mathbf{0}_{N_b-2+i} & \mathbf{n}_f \end{bmatrix} \quad \mathbf{n}_1 = \begin{bmatrix} 1 \\ \mathbf{0}_{N_b-i} \end{bmatrix} \quad \mathbf{n}_f = \begin{bmatrix} 1 \\ \mathbf{0}_{N_b-2+i} \end{bmatrix} \tag{19b}$$

where $\mathbf{n}$ and $\mathbf{0}_v$ are defined as in (18). Notice the first and final block $(\mathbf{n}_1, \mathbf{n}_f)$ are shrinking and expanding, respectively. This parameterisation is then applied sequentially $i = 1 \rightarrow N_b$ until the first block reaches its limit, and resets to its original size ($i = 1$).

By substituting the MWB input parameterisation in the standard quadratic program (17), the application of the MWB approach then leads to formulating and solving N_b different quadratic programs sequentially and repeating infinitely $i = 1 \rightarrow N_b, 1 \rightarrow N_b, 1 \rightarrow \cdots$ as the horizon moves forward defined as:

$$J = \frac{1}{2}\Delta\hat{\mathbb{U}}^T E_{\mathbb{N}}^{[i]}\Delta\hat{\mathbb{U}} + \Delta\hat{\mathbb{U}}^T f_{\mathbb{N}}^{[i]} \quad s.t. \quad M_{\mathbb{N}}^{[i]}\Delta\hat{\mathbb{U}} \leq b \tag{20a}$$

$$E_{\mathbb{N}}^{[i]} = \mathbb{N}_i^T H^T Q H \mathbb{N}_i = \mathbb{N}_i^T E \mathbb{N}_i \tag{20b}$$

$$f_{\mathbb{N}}^{[i]} = \mathbb{N}_i^T H^T Q(Gx_k + H_w\hat{U}_w) = \mathbb{N}_i^T f \tag{20c}$$

$$M_{\mathbb{N}}^{[i]} = \begin{bmatrix} \mathbb{N}_i \\ -\mathbb{N}_i \\ D\mathbb{N}_i \\ -D\mathbb{N}_i \end{bmatrix} \quad b = \begin{bmatrix} \Delta u_{max}\mathbf{1} \\ -\Delta u_{min}\mathbf{1} \\ (u_{max} - u_{k-1})\mathbf{1} \\ (-u_{min} + u_{k-1})\mathbf{1} \end{bmatrix} \tag{20d}$$

where $E_{\mathbb{N}}^{[i]} \in \mathbb{R}^{N_u \times N_u}$ is the "compressed" Hessian, which can be pre-stored for faster computations. On the other hand, the "compressed" linear term $f_{\mathbb{N}}^{[i]} \in \mathbb{R}^{N_u}$ can also be pre-stored by separating the values in $f_{\mathbb{N}}^{[i]} = f_{1_{\mathbb{N}}}^{[i]} x_k + f_{2_{\mathbb{N}}}^{[i]}\hat{U}_w$ with $f_{1_{\mathbb{N}}}^{[i]} = \mathbb{N}_i^T H^T Q G$ and $f_{2_{\mathbb{N}}}^{[i]} = \mathbb{N}_i^T H^T Q H_w$. Moreoever, it is trivial to derive that when using the blocking matrix $\mathbb{N}_i$ as defined in (19), the constraint matrix have redundant zero rows $\forall\ i$, and can be reduced to,

$$M_{\mathbb{N}}^{[i]} = M_{\mathbb{N}} = \begin{bmatrix} I_{\mathbb{N}} \\ -I_{\mathbb{N}} \\ D_{\mathbb{N}} \\ -D_{\mathbb{N}} \end{bmatrix} \quad b_{\mathbb{N}} = \begin{bmatrix} \Delta u_{max}\mathbf{1}_{\mathbb{N}} \\ -\Delta u_{min}\mathbf{1}_{\mathbb{N}} \\ (u_{max} - u_{k-1})\mathbf{1}_{\mathbb{N}} \\ (-u_{min} + u_{k-1})\mathbf{1}_{\mathbb{N}} \end{bmatrix} \tag{21}$$

where $M_{\mathbb{N}} \in \mathbb{R}^{4N_u \times N_u}$ is the "reduced" constraint matrix, $b_{\mathbb{N}} \in \mathbb{R}^{4N_u}$ is the "reduced" constraint vector, $I_{\mathbb{N}} \in \mathbb{R}^{N_u \times N_u}$ is an identity matrix, $D_{\mathbb{N}} \in \mathbb{R}^{N_u \times N_u}$ is a lower triangular matrix, and $\mathbf{1}_{\mathbb{N}} \in \mathbb{R}^{N_u}$ is column-vector of ones, all of which have reduced dimensions $N_u = \lceil \frac{N_p}{N_b} \rceil$ when compared to the original constraint terms (17c), thus can lead to significant computational benefits as discussed in the results section 4. Once the optimisation is solved, the original decision vector can be recovered using (19).

4. RESULTS

In this section, we present the simulation results of the control of a point-absorber WEC using F-DoF MPC, GPC and the proposed Moving Window Blocking (MWB) MPC approach. The WEC model considered is a heaving semi-submerged sphere reacting against a fixed reference (see Fig. 1), with a radius of 5 m and draft of 5 m, mass $m = 2.6831 \times 10^5$ kg placed in deep water. A sampling time of $T_s = 0.1s$ was used. The hydrodynamic coefficients were computed using the open source *NEMOH* (Penalba et al., 2017). The convolution integral in the radiation force (5) is approximated by a state-space model of order 6 (See (7)). Here, the state-space matrices A_r, B_r, and C_r are computed using the toolbox *FOAMM*, which is based in the moment-matching method (Faedo et al., 2018). The resulting state space matrices for the discretised model of (10) are given by (22). The Matlab code and results presented in this paper are available through a Code Ocean compute capsule `https://doi.org/10.24433/CO.0481002.v1` (Guerrero-Fernandez and Gonzalez Villarreal, 2019).

To focus on the comparison of the control strategies, which is the main driver of this study, perfect knowledge of the future wave forces $\hat{U}_w$ and state x_k is considered during the simulation time. The wave elevation of the irregular sea wave was built using the JONSWAP (Joint North Sea Wave Project) spectrum discretised in frequency between 0.02 Hz to 0.80 Hz, corresponding to 1.25 s to 50 s periods respectively, with a frequency step of $\Delta f = 5.2 \times 10^{-3}$ Hz. Considering a significant wave height $H_0 = 2.0$ m and wave peak period $T_p = 10.0$ s. Fig. 3 shows the resulting excitation force on the buoy, with a force range from 8.7119×10^5 N to -8.5133×10^5 N.

Here, for comparison purpose, Full-Degrees Of Freedom (F-DoF) MPC strategy is considered as the control strategy which delivers the maximum possible extracted energy (100% efficiency). For the optimisation setup, a prediction horizon of 10 s ($N_p = 100$) was used with a block size of $N_b = 5$ for the MWB approach which resulted in $N_u = 20$ decision variables. To perform a fair comparison, the GPC approach used the same amount of decision variables compressed at the beginning of the prediction horizon. Moreover, matrix B_d of (22) was re-scaled/normalized to avoid numeric conditioning problems of the optimisation. Finally, constraints on the input and input increment were considered as $||u_{k+i}|| \leq 200kN$ and $||\Delta u_{k+i}|| \leq 200kN\ \forall\ i = [0, N_p - 1]$, respectively.

Fig. 4 shows the energy extracted for the different controllers studied in this paper, and the final value of the energy extracted at the end of the 600 s simulation is shown in Table 1. The results show that the proposed MWB approach offers almost the same amount of energy compared to the maximum feasible (F-DoF MPC), with an efficiency of 98.79 %. On the other side GPC is ranked third in the amount of energy extracted, with an efficiency of 92.84 %. Moreover, Zoom *A* in Fig. 4, shows the bidirectional reactive power flowing between the PTO and the absorber, condition required for the active control strategies to maximise the extracted energy (Pecher and Kofoed, 2017).

On an interesting note, it can be seen that F-DoF unconstrained MPC with input saturation failed to extract energy altogether as seen in Table 1. Similar results were obtained in Li and Belmont (2014). An alternative is to add an extra quadratic penalization term on the input of the form ($J_\lambda = J + \lambda \sum u_{k+i-1}^2\ \forall\ i = [1, N_p]$) to the cost function (12a) as discussed in Li and Belmont (2014), however, this causes disagreements between the optimisation terms, inevitable leading to suboptimalities. To perform a fair comparison, a brute-force search was performed to select the value of $\lambda = 1.12$ which achieved the highest energy absorption for the unconstrained penalised (λ) F-DoF MPC solution with an efficiency of 88.71, thus still resulting in worse performance than both, GPC and MWB.

Table 1. Energy Extracted for 600 s simulation using F-DoF MPC, MWB MPC, GPC and F-DoF Unconstrained MPC (with and without additional λ penalization terms)

Method	Energy extracted [MJ]	Efficiency [%]
F-DoF MPC	306.974	100
F-DoF Unc. MPC	−328.738	LOSS
F-DoF Unc. MPC (λ)	272.318	88.71
MWB MPC	303.274	98.79
GPC	285.000	92.84

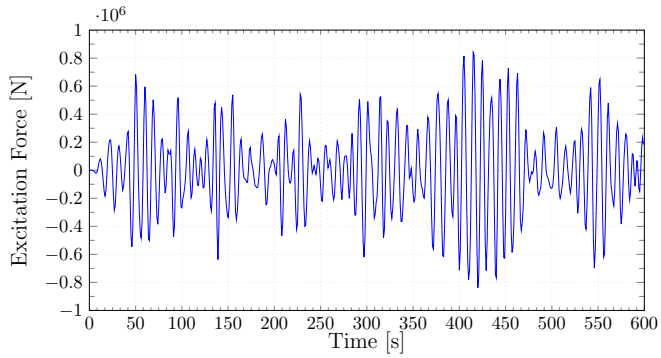

Fig. 3. Excitation force u_{exc} for a irregular sea condition built using the JONSWAP spectrum, with wave height $H_0 = 2.0\,\text{m}$ and wave peak period $T_p = 10.0\,\text{s}$

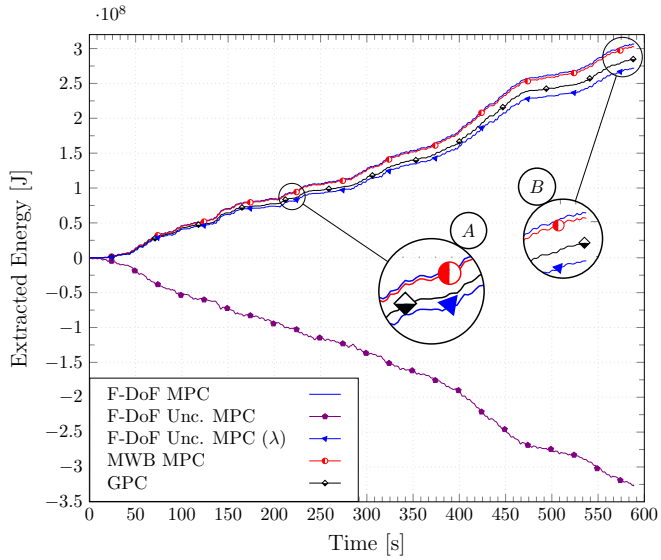

Fig. 4. Energy Extracted tendency for 600 s simulation using F-DoF MPC, MWB MPC, GPC and F-DoF Unconstrained MPC (with/without λ terms)

Fig. 2 shows the predicted trajectories of the buoy position and the control input u for the three MPC solutions, namely: the F-DoF MPC, the MWB and the GPC. From the lower plot of Fig. 2, it can clearly be seen how the MWB approach embeds the blocked parameterisation, distributing the decision variables along the prediction horizon with the sequential shrinking approach (first block size of $4 \rightarrow i = 2$) visible in the zooms A and B, respectively. In contrast, in the GPC approach, all the decision variables are calculated for the beginning of the prediction horizon and kept constant after a certain time which leads to a significant difference in the predicted trajectory of the control action.

On the other hand, the predicted trajectories of the buoy position can be seen in the upper plot of Fig. 2 where the solutions for both, F-DoF MPC and MWB MPC, are practically indistinguishable, with negligible differences visible in zooms a, b and c. This visual agreement is supported by the efficiency given in Table 1. In contrast, this can not be said about the GPC solution, where one can see the significant differences in the predicted trajectories, most likely related to the differences in the available control action trajectories. In simple terms, the GPC strategy is unable to replicate the position trajectory when using the same number of decision variables compressed in the beginning of the prediction horizon.

With regard to the computation times used to solve the optimal problem at each time step, Table 2 summarises relevant optimisation statistics of each method employed in this study when using the interior point method of Matlab R2018b "quadprog" function in a normal PC with an Intel i5-7500 @ 3.4 GHz CPU, and 8 GB @ 2.4 GHz DDR4 RAM. On average, the proposed MWB approach makes it possible to solve the optimal problem 12.6 times faster compared to the F-DoF MPC. The reason for this gain in the computation time is due to the fact that, in this case, the number of decision variables and constraints are reduced by 5 times ($N_b = 5$), i.e., from $N_p = 100$ to $N_u = 20$ decision variables, and from $4N_p = 400$ to $4N_u = 80$ constraints, which ultimately leads to faster and lower amount of iterations required by the QP to solve the problem. Similar comments of the timing statistics can be made for the GPC strategy, with the main drawback being a performance degradation (efficiency of 92.84 %). Also, it can be seen that the MWB provides the smallest standard deviation for both average timing statistics, thus leading to an optimisation with more consistent/repeatable behaviour.

Table 2. Statistics of the Optimisation

Method	Avg. opt. time [ms]	Avg. num. of QP iterations	Avg. opt. time per iter. [ms]	Gain
F-DoF MPC	19.78 ± 2.75	8.19 ± 0.79	2.42 ± 0.27	-
MWB MPC	1.58 ± 0.23	6.75 ± 0.98	2.37 ± 0.04	12.6
GPC	1.39 ± 0.51	7.37 ± 1.17	1.93 ± 0.10	14.2

Finally, it should be pointed out that the main contribution of the MWB approach is not merely the reduction in the computation time required to solve the OCP at each sampling time, but the ability to retain almost the same performance than that of F-DoF via the shifting input parameterisation, a property that GPC does not deliver. Results provided in Tables 1 and 2 support this.

$$A_d = \begin{bmatrix} 0.9905 & 0.0997 & -0.0003 & -0.0002 & 0.0003 & 0.0004 & -0.0005 & 0.0015 \\ -0.1896 & 0.9899 & -0.0048 & -0.0049 & 0.0057 & 0.0084 & -0.0096 & 0.0297 \\ -0.0253 & 0.2166 & 0.7789 & 0.2342 & -0.2682 & 0.1451 & -0.2394 & 0.1985 \\ -0.0021 & 0.0171 & -0.0373 & 1.0167 & -0.0214 & 0.0111 & -0.0190 & 0.0156 \\ -0.0361 & 0.3052 & -0.3113 & 0.3019 & 0.5081 & 0.6650 & -0.3376 & 0.2792 \\ 0.0013 & -0.0474 & 0.0476 & -0.0472 & -0.4112 & 0.8425 & 0.0486 & -0.0465 \\ -0.0217 & 0.1850 & -0.1887 & 0.1830 & -0.2292 & 0.1236 & 0.7820 & 0.3332 \\ 0.0015 & -0.0201 & 0.0203 & -0.0199 & 0.0232 & -0.0160 & -0.1424 & 0.9675 \end{bmatrix} \quad B_d = \begin{bmatrix} 0.0123 \\ 0.2465 \\ 0.0329 \\ 0.0028 \\ 0.0469 \\ -0.0017 \\ 0.0282 \\ -0.0019 \end{bmatrix} \cdot 10^{-6} \quad C_d = \begin{bmatrix} 1 & 0 \\ 0 & 1 \\ 0 & 0 \\ 0 & 0 \\ 0 & 0 \\ 0 & 0 \\ 0 & 0 \\ 0 & 0 \end{bmatrix}^T \tag{22}$$

5. CONCLUSION

The control strategies presented in this study are intended to maximise the energy production of a generic point-absorber wave energy converter subject to input and input rate constraints related to physical limits. The system benefits from the ability of Model Predictive Control to include future information of both wave forces and physical constraints. Moreover, to reduce the computational burden, it uses Moving Window Blocking approach where the decision variables are parameterised through a set of input-blocking matrices which result in a sequence of Quadratic Programs of reduced size to be solved sequentially and repeating infinitely. This allows solutions up to 12.52 times faster with efficiency as low as 98.8 % when compared to the Full Degrees of Freedom MPC optimal solution. Although both, the F-DoF MPC and the proposed MWB MPC approach are computationally feasible for this particular single WEC device model, the proposed control strategy could be a key methodology for implementing Centralised Model Predictive Control for wave farms. The solution of the proposed approach was further compared with GPC, as well as with two versions of Unconstrained F-DoF MPC, one of which was shown to result in a complete loss of energy extraction.

Future work will include the assessment of the solution using real-time embedded hardware such as FPGAs, as well as faster QP solvers such as QP OASES. Moreover, the application will be extended to wave farms using a centralised optimisation framework, and compared with decentralised/distributed approaches as well as with other parameterisation such as collocation points based on pseudospectral methods. Finally, the mathematical models and MPC formulation will be extended to the nonlinear case, and will include further modeling such as actuator dynamics and future wave force predictions.

Ultimately, enhancing peer collaboration and transparency, the findings provided in this paper and the Matlab code used in the simulation are accessible through a Code Ocean capsule (`https://doi.org/10.24433/CO.0481002.v1`) (Guerrero-Fernandez and Gonzalez Villarreal, 2019).

ACKNOWLEDGEMENTS

The first author would like to acknowledge the support of MICITT (Ministerio de Ciencia, Tecnología y Telecomunicaciones) of Costa Rica, who funded this work through a scholarship under the contract MICITT-PINN-CON-2-1-4-17-1-027. The second author would like to acknowledge the support of CONACyT, Mexico.

REFERENCES

Cagienard, R., Grieder, P., Kerrigan, E.C., and Morari, M. (2007). Move blocking strategies in receding horizon control. *Journal of Process Control*, 17(6), 563–570.

Cretel, J., Lewis, A.W., Lightbody, G., and Thomas, G.P. (2010). An application of Model Predictive Control to a wave energy point absorber. *IFAC Proceedings Volumes (IFAC-PapersOnline)*, 1, 267–272.

Cretel, J.A., Lightbody, G., Thomas, G.P., and Lewis, A.W. (2011). Maximisation of energy capture by a wave-energy point absorber using model predictive control. In *Proceedings of the 18th World Congress The International Federation of Automatic Control*, 3714–3721. IFAC, Milano, Italy.

Cummins, W. (1962). The impulse response fitting and ship motions. Technical report, Institut fuer Schiffbau der Universitaet, Hamburg, Hamburg.

Faedo, N., Olaya, S., and Ringwood, J.V. (2017). Optimal Control, MPC and MPC-Like Algorithms for Wave Energy Systems: An Overview. *IFAC Journal of Systems and Control*.

Faedo, N., Peña-Sanchez, Y., and Ringwood, J.V. (2018). Finite-order hydrodynamic model determination for wave energy applications using moment-matching. *Ocean Engineering*, 163, 251–263.

Garcia-Violini, D. and Ringwood, J.V. (2019). Energy maximising robust control for spectral and pseudospectral methods with application to wave energy systems. *International Journal of Control*, 1–12.

Guerrero-Fernandez, J. and Gonzalez Villarreal, O.J. (2019). Model Predictive Control for Wave Energy Converters: A Moving Window Blocking Approach. Code Ocean. Available in https://doi.org/10.24433/CO.0481002.v1.

H.J.Ferreau, H.G. Bock, M.D. (2008). An online active set strategy to overcome the limitations of Explicit MPC. *International Journal of Robust and Nonlinear Control*, 18(October 2014), 816–830.

International Energy Agency (2019). Electricity Information: Overview. Technical report, International Energy Agency. URL `https://webstore.iea.org/`.

Li, G. and Belmont, M.R. (2014). Model predictive control of sea wave energy converters - Part I: A convex approach for the case of a single device. *Renewable Energy*, 69, 453–463.

Mørk, G., Barstow, S., Kabuth, A., and Pontes, M.T. (2010). Assessing the global wave energy potential. In *Proceedings of the International Conference on Offshore Mechanics and Arctic Engineering - OMAE*, volume 3, 447–454. ASME.

Pecher, A. and Kofoed, J.P. (2017). *Handbook of Ocean Wave Energy*. Springer.

Penalba, M., Cortajarena, J.A., and Ringwood, J. (2017). Validating a Wave-to-Wire Model for a Wave Energy Converter—Part II: The Electrical System. *Energies*, 10(7), 1002.

Pérez, T. and Fossen, T.I. (2008). Time-vs. frequency-domain Identification of parametric radiation force models for marine structures at zero speed. *Modeling, Identification and Control*, 29(1), 1–19.

Roessling, A. and Ringwood, J.V. (2015). Finite order approximations to radiation forces for wave energy applications. *Renewable Energies Offshore*, 359–366.

Rossiter, J. (2018). *A first course in predictive control*. CRC Press.

Sheng, W. (2019). Wave energy conversion and hydrodynamics modelling technologies: A review. *Renewable and Sustainable Energy Reviews*, 482–498.

Wang, L. (2004). Discrete model predictive controller design using Laguerre functions. *Journal of Process Control*, 14(2), 131–142.

Yu, Z. and Falnes, J. (1995). State-space modelling of a vertical cylinder in heave. *Applied Ocean Research*, 17(5), 265–275.